LANGMUIR

pubs.acs.org/Langmuir Article

Impact of the Undersaturation Level on the Longevity of Superhydrophobic Surfaces in Stationary Liquids

Ali Nosrati, Shabnam Mohammadshahi, Mehdi Raessi, and Hangjian Ling*

Cite This: https://doi.org/10.1021/acs.langmuir.3c03006 Read Online

ACCESS | Metrics & More | Article Recommendations | Supporting Information

ABSTRACT: Although the longevity of superhydrophobic surface (SHS) induced by diffusive gas transfer has been extensively studied, the scaling relation between SHS longevity and undersaturation level of the liquid is still an open question. In this study, we address this question by performing experiments where the plastron decay is visualized by a nonintrusive optical technique based on light reflection, the gas diffusion is introduced by using liquid with low dissolved gas concentrations, and the SHS longevity is measured based on the status of gas on the entire surface. We find that the SHS longevity (t_f) follows a scaling relation: $t_f \sim (1 - s)^{-2}$, where s is the ratio of the gas concentration in liquid to that in the plastron. This scaling relation implies that as the gas is dissolving into the liquid, mass flux J reduces with time as $J \sim t^{-0.5}$. Furthermore, we find that the diffusion length L_D reduces as the undersaturation level increases, following the scaling relation of $L_D \sim (1 - s)^{-1}$. Lastly, we show that an SHS with a greater texture depth has a longer longevity and a larger L_D. Our results provide a better understanding of SHS longevity in undersaturated liquid.

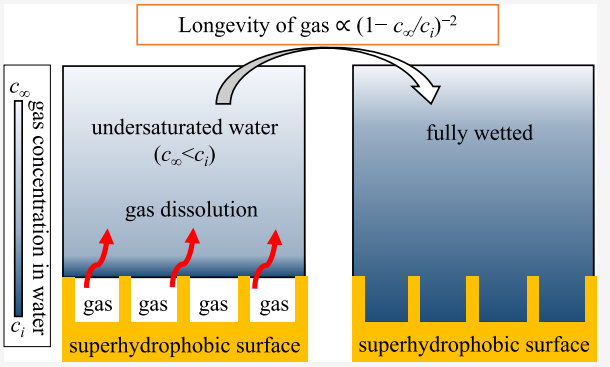

INTRODUCTION

Superhydrophobic surface (SHS) is an emerging material with many applications such as drag reduction,[1,2] anticorrosion,[3,4] antibiofouling,[5−7] anti-icing,[8−10] energy harvesting,[11,12] and biosensing.[13,14] Most of these applications rely on the presence of micro/nanoscale gas bubbles trapped within the surface texture when the SHS contacts with liquid. However, the beneficial gas trapped on a SHS can slowly dissolve in the ambient liquid, shortening the longevity of SHS.[15] In the past two decades, significant attention has been paid to the SHS longevity in undersaturated environments.[16] Experimental studies measured the SHS longevity by technologies such as total internal reflection (TIR),[17−24] brightfield imaging,[25−27] confocal microscopy,[28−31] X-ray diffraction,[32] and reflection interference contrast microscopy (RICM).[33] Fluorescence microscopy was used to measure the spatial distribution of gas concentration in flows over a SHS.[34] Numerical investigations simulated the gas dissolution process by assuming a fixed invasion coefficient,[35−39] or solving the gas diffusion equation[40−42] or the coupled mass and momentum transport equations,[34,43,44] or using an approximate integral method.[45] Various parameters were considered, including pressure,[17,19,28] gas concentration in liquid,[26] flow Reynolds number,[23,24] and SHS texture.[35,36,39,46] Theoretical models were proposed to predict the longevity of SHSs in a stationary liquid[28,41] and to estimate the Sherwood number (the dimensionless mass transfer rate) for laminar and turbulent flows over SHSs.[27,31,45]

Despite the past extensive studies, there is an open question on the scaling relation between SHS longevity and the undersaturation level of the liquid. Although it is well-known that the SHS longevity reduces with an increasing undersaturation level, understanding the scaling relation between the two quantities is critical for the accurate prediction of SHS longevity. The gas concentrations in the bulk liquid and at the gas−liquid interface are denoted by c_∞ and c_i, respectively. The gas transfer from a SHS to liquid is driven by the gradient of gas concentration near the interface when $c_i > c_\infty$. The undersaturation level of the liquid is defined as $s = c_\infty/c_i < 1$. A liquid with a smaller value of s is more undersaturated. Previous studies introduced undersaturation conditions by either increasing pressure in the liquid (where c_i increases following Henry's law and pressure balance at gas−liquid interface) or reducing the gas concentration in liquid. Using confocal microscopy to measure the SHS longevity, Lv et al.[28] reported that the SHS longevity is proportional to $(1 - s)^{-1}$. However, by numerically solving the gas diffusion equation, Bourgoun and Ling[41] proposed that the SHS longevity is

Received: October 6, 2023
Revised: November 10, 2023
Accepted: November 13, 2023

proportional to $(1 - s)^{-2}$. Other experiments[17,19,26] measured the SHS longevity under a range of s, but did not report the scaling relationship between them.

The goal of this study is to address this open question by collecting new experimental data on the SHS longevity in liquids with different values of s. In particular, we aim to assess the two scaling relations proposed by Lv et al. and Bourgoun and Ling, and identify the one that best captures the SHS longevity in undersaturated environments. Our experiments are distinct from those by Lv et al. in several ways. First, unlike Lv et al. where a water-immersion objective was placed very close to the SHS, we apply a nonintrusive optical method that does not disturb the gas diffusion process. Second, contrary to Lv et al., who used a very small portion of a large SHS to determine its longevity, we measure the entire SHS to address the influence of uneven gas diffusion rate at different regions of the SHS.[17,26] Lastly, unlike Lv et al., who introduced the undersaturation condition by increasing pressure, we induce the gas diffusion by using liquid with a low dissolved gas concentration so that the stability of SHS is not affected by pressure.[47]

MATERIALS AND METHODS

This study considers three SHSs, two have an array of microholes, as shown in Figure 1a,b, and one with an array of microposts, as shown in Figure 1c. Holes and posts on each of the SHSs have a radius of r = 30 μm and a wavelength of λ = 100 μm. The depth of the holes is h = 46 and 61 μm for the two SHSs with holes, respectively, and the height of the posts is h = 61 μm. These texture parameters are selected so that the gas trapped on the SHS (or Cassie–Baxter state) is thermodynamically stable.[48] The reason to include three SHS samples is to ensure that the observed trends are consistent among different samples, and the proposed scaling relation is applicable to SHSs of various texture geometries. Furthermore, the reason for choosing relatively simple texture geometries, such as holes and posts, is because they have well-defined texture geometries, simplifying the calculation of the amount of gas on SHS. The three SHSs are fabricated on a PDMS [poly(dimethylsiloxane)] surface by standard soft-lithography.

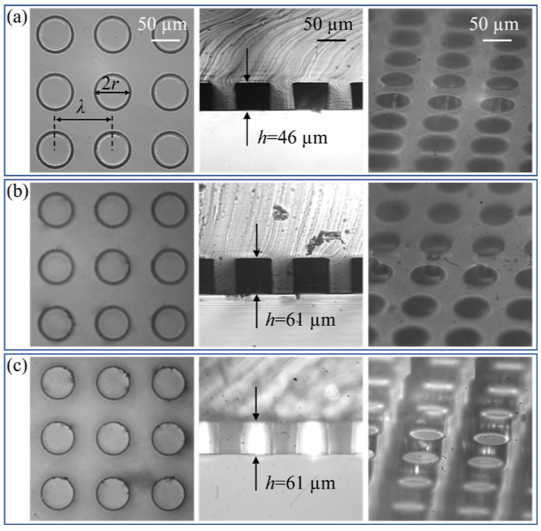

Figure 1. Top (left column), cross-section (center), and tilted views (right) for three SHS samples used in this study: SHS with holes of (a) 46 μm and (b) 61 μm depth, and (c) SHS with posts of 61 μm height. Scale bar shown in (a) applies to all images.

Figure 2a shows a schematic of our experimental setup. The experiments are carried out in a fully closed tube, which has a length of 270 mm and a diameter of 12.5 mm. The tube is maintained at atmospheric pressure P_{atm} and room temperature (20 ± 1 °C). The tube length is made sufficiently long that gas diffusion occurs freely within the tube in the vertical direction. The SHS of 12.5 mm diameter (the same diameter of the tube) is mounted at the top end of the tube. The reason for installing the SHS at the top of the tube is to have P_{atm} just below the SHS.

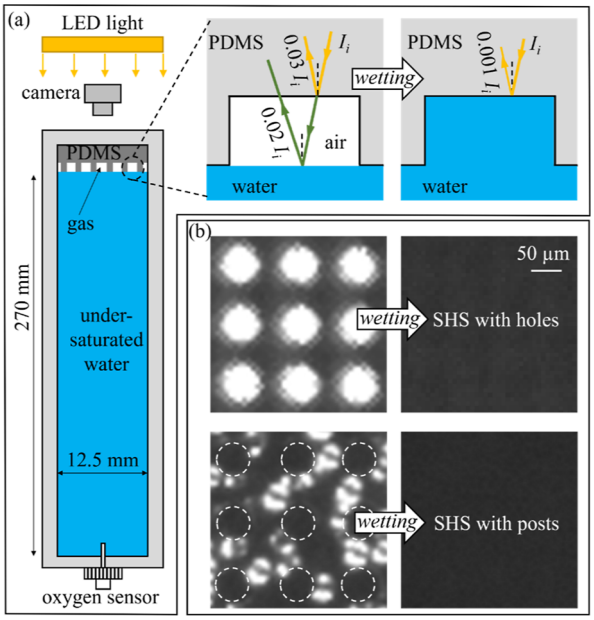

Figure 2. (a) Schematic of experimental setup for measuring SHS longevity in undersaturated liquid (not to scale); and (b) four sample recorded images correspond to partially wetted SHSs initially trapping air, shown as bright spots, and SHSs at fully wetted state. Posts on the SHS are highlighted by dashed lines.

In this study, the gas trapped on the SHS is air, and the liquid in the tube is deionized (DI) water. The air concentration in water when saturated at P_{atm} and 20 °C is $c_{ref} = P_{atm}/k_H$ = 0.023 kg/m^3,[49] where k_H is the Henry's law constant. Assuming the air–water interface on the SHS is flat at the beginning of the gas dissolution process, the pressure in the plastron is P_{atm}, and the air concertation at the gas–liquid interface is $c_i = c_{ref}$. When the interface deforms due to the transfer of gas into the liquid, the pressure in the plastron can change by a maximum value[47] of $\Delta p^{max} = |2\gamma \cos \theta_{adv}/r| = 668$ Pa, where $\theta_{adv} = 98°$ denotes the local advancing contact angle for PDMS (the value 98° is selected based on the experimental measurements by Moulinet and Bartolo[50]) and γ = 72 mN/m is the surface tension of water. Note that θ_{adv} is the maximum contact angle that can be reached by the air–water interface and is a material property that does not change during the wetting process. Consequently, according to Henry's law, due to Δp^{max}, c_i changes by an amount less than $0.01c_{ref}$. Thus, it is safe to consider c_i as a constant in our study.

To induce the gas diffusion, we vary c_∞ in the range $0.35c_i$ to $0.9c_i$ (so that s varies from 0.35 to 0.9). To achieve this, we leave the water in an open container under vacuum for 20 min to 24 h (depending on the desired s) before each experiment. The value of c_∞ is measured by an optical oxygen sensor (FirestingO2, Pyro Science) connected to the bottom of the tube. We monitored c_∞ continuously throughout the experiments. The value of c_∞ changes by less than 1% during each measurement which lasts for a maximal duration of 30 h. This confirms that our experimental facility is airtight, and the gas diffusion process is not affected by the bottom boundary. Moreover, to ensure that no excess air is trapped on the SHS or on the tube walls during the experiments, we use the following experimental procedure. First,

https://doi.org/10.1021/acs.langmuir.3c03006
Langmuir XXXX, XXX, XXX–XXX

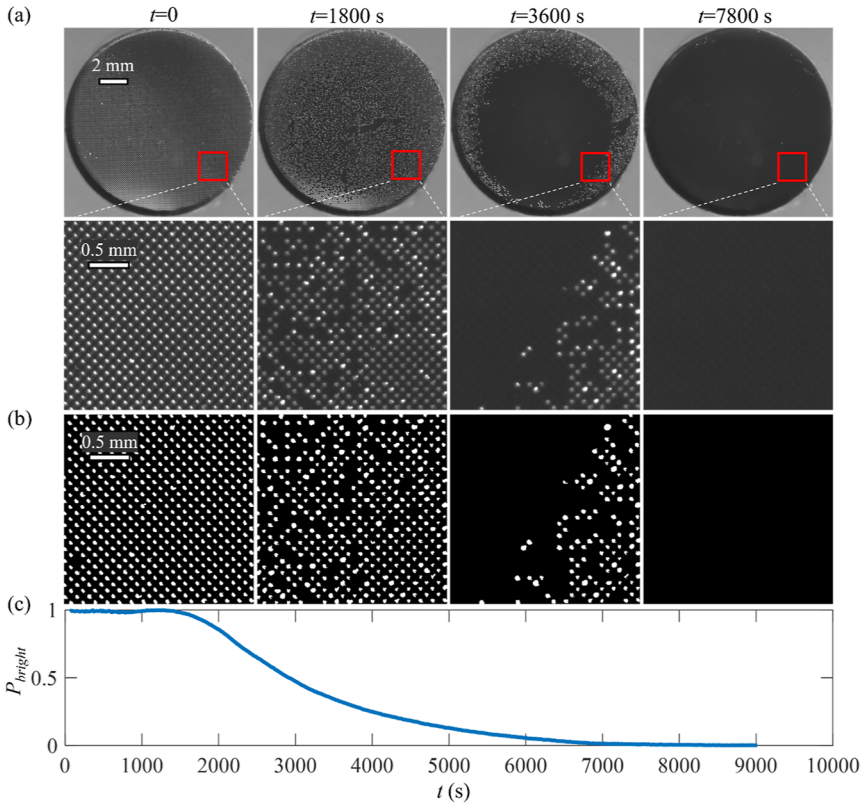

Figure 3. (a) Time-series of images recorded during a typical gas diffusion process for SHS with holes (h = 46 μm) and at s = 0.8 along with magnified views; (b) binarized images corresponding to those shown in (a); and (c) time variation of P_{bright} corresponding to the case shown in (a).

the undersaturated water is slowly added to the tube while keeping the tube nearly vertical until the water overflows. Then, we gently shake the tube to allow air bubbles attached on the tube walls (if there are any) to rise and escape. Finally, we placed the SHS sample on top of the water surface, followed by sealing the tube by installing a glass plate on the back of the SHS sample. The presence of any excess air bubbles on the SHS can be visually checked during the experiment, and if excess air is detected, we exclude such data from our analysis.

Figure 2a also shows the optical arrangement for measuring the status of gas on the SHS. An LED light positioned above the tube illuminates in the direction perpendicular to the sample, and a CMOS camera (FLIR Grasshopper 3, pixel size of 5.5 mm, 2048 × 2048 pixels) located on the same side is used to record the light reflected from the SHS. The LED light does not change the temperature of the liquid as confirmed by a temperature sensor. In addition, Figure 2a illustrates the principle of the optical measurement system. As the light encounters the SHS, a small portion of the light is reflected. For normal incidence, the ratio of reflected light intensity (I_r) to incident light intensity (I_i) is given by

$$\frac{I_r}{I_i} = \left(\frac{n_2 - n_1}{n_2 + n_1}\right)^2 \quad (1)$$

where n_1 and n_2 are the refractive indexes of the media on two sides of the interface. Given the refractive indexes of air, water, and PDMS are 1.0, 1.33, and 1.43, respectively, the intensities of lights reflected from the air−water interface, air−PDMS interface, and PDMS−water interface are 0.02I_i, 0.03I_i, and 0.001I_i, respectively. Therefore, the intensity of light reflected from the region where gas is entrapped is about 50 times larger than that reflected from the region where there is no gas. This is clearly demonstrated by the four sample images captured in our experiments, as shown in Figure 2b. Note that only a small portion of the recorded image is shown in Figure 2b for illustration purposes. When the gas is entrapped on the surfaces (at the beginning of experiments), most of the areas covered by gas is bright. In contrast, when the SHSs are fully wetted (at the end of the experiments), the images are much darker.

The current optical setup ©s very"©im'lar to the RICM since both record two light beams reflected from the air−water interface and from the air−PDMS interface. For RICM, an objective lens is inserted before the camera and an interference between the two reflected lights is recorded. Kim and Park[33] analyzed the interference pattern and tracked the motion of the air−water interface. In the present study, our goal is to capture the entire SHS so that the nonuniform gas diffusion across the surface can be accounted. Thus, we did not use an objective lens. Our image area is 14.6 × 14.6 mm^2, slightly larger than the size of the SHS to cover the entire sample. Due to the low spatial resolution, as shown in Figure 2b, we did not observe an interference between the two reflected lights. We recorded data at 0.1 frame per second in all our experiments.

RESULTS AND DISCUSSION

Figure 3a shows a time series of images recorded of a SHS with holes during a typical gas dissolution process. Initially at t = 0, the SHS has a uniform array of bright spots, suggesting that all the microholes on the SHS are filled with air. As time progresses and air is dissolved into the water, more and more bright spots on the SHS diminish and become dark, as shown by images at t = 1800 and 3600 s. The bright-to-dark transition of individual spots indicates that air trapped within the corresponding holes has been dissolved in the water. Finally, at t = 7800 s, almost all bright spots disappear, suggesting that the entire SHS is fully wetted. Although the SHS has a uniform pattern, some regions of the SHS transition to the dark quicker than others. Such nonuniform wetting rate over a SHS with a regular pattern was also observed in other experimental studies.[17,26] The possible reasons include the initial dis-

https://doi.org/10.1021/acs.langmuir.3c03006
Langmuir XXXX, XXX, XXX−XXX

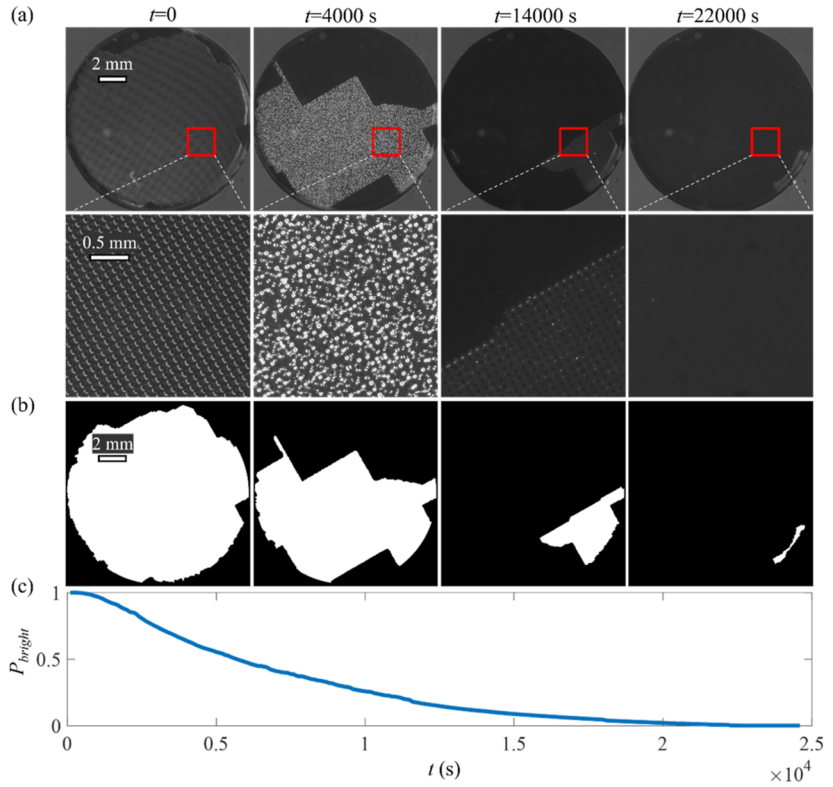

Figure 4. (a) Time-series of images recorded during a typical gas diffusion process for SHS with posts and at $s = 0.8$ along with magnified views; (b) binarized images corresponding to those shown in (a); and (c) time variation of P_{bright} corresponding to the case shown in (a).

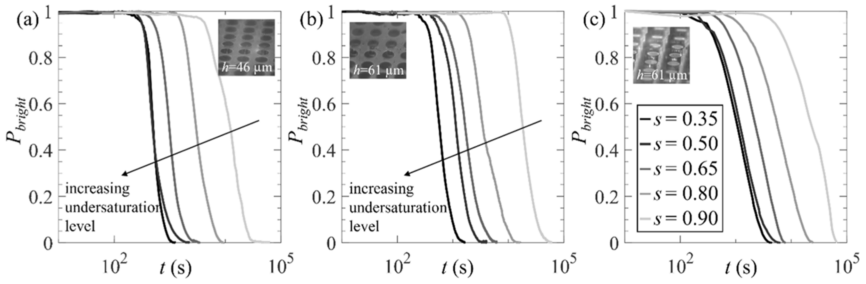

Figure 5. Time variations of P_{bright} at different values of s for SHSs with holes of (a) 46 μm and (b) 61 μm depth and (c) SHS with posts of 61 μm height.

turbance in the liquid caused during installation of the SHS and dust particles attached on the SHS.

To minimize the measurement error introduced by the nonuniform wetting rate, we determine the SHS longevity based on the gas status of the entire SHS. First, we count the number of bright spots N_{bright} on the recorded images by converting the raw images into binary images, as shown in Figure 3b, and measuring N_{bright} based on the number of white objects on the binary images. Then, we define the percentage of bright spots as $P_{bright}(t) = N_{bright}(t)/N_{bright}(t = 0)$. Figure 3c shows the time-variation of P_{bright} corresponding to the case shown in Figure 3a. At the initial period of gas diffusion process ($t < 1000$ s), P_{bright} remains nearly constant at 1. This is because most of the holes are still partially filled by gas and in a metastable state.[28] According to the principle of light reflections described above, the intensity of light reflected from a hole partially filled with gas is similar to that from a hole that is fully filled with gas. Finally, the SHS longevity (t_f) is estimated based on the time when P_{bright} reaches a threshold value (e.g., $P_{bright} = 0.1$, meaning 90% of the holes on SHS are fully wetted and the surface almost loses its functionality). This data analysis approach for determining SHS longevity is similar to the one used by Bobji et al.[17] who visualized the plastron by the TIR technique.

Next, a typical wetting transition for the SHS with posts caused by gas dissolution is shown in Figure 4a. Similar to the trend seen in Figure 3a, the area of the bright region decreases with time, indicating the dissolution of gas into the liquid. However, contrary to the SHS with holes where individual gas pockets are isolated from each other, for SHS with posts, the gas between different posts is connected, creating a single initially large dry region, as seen on the images. Moreover, the boundaries between the wet and dry regions mostly consist of straight lines (e.g., images shown at $t = 4000$ and 14,000 s). To estimate the SHS longevity, we convert the raw images in Figure 4a to binarized images, as shown in Figure 4b, and calculate the percentage of surface area that is bright as $P_{bright}(t) = A_{bright}(t)/A_{bright}$ ($t = 0$), where A_{bright} indicates the area of the bright region in Figure 4b. Figure 4c shows the time-variation of P_{bright} for the case corresponding to Figure 4a.

https://doi.org/10.1021/acs.langmuir.3c03006
Langmuir XXXX, XXX, XXX−XXX

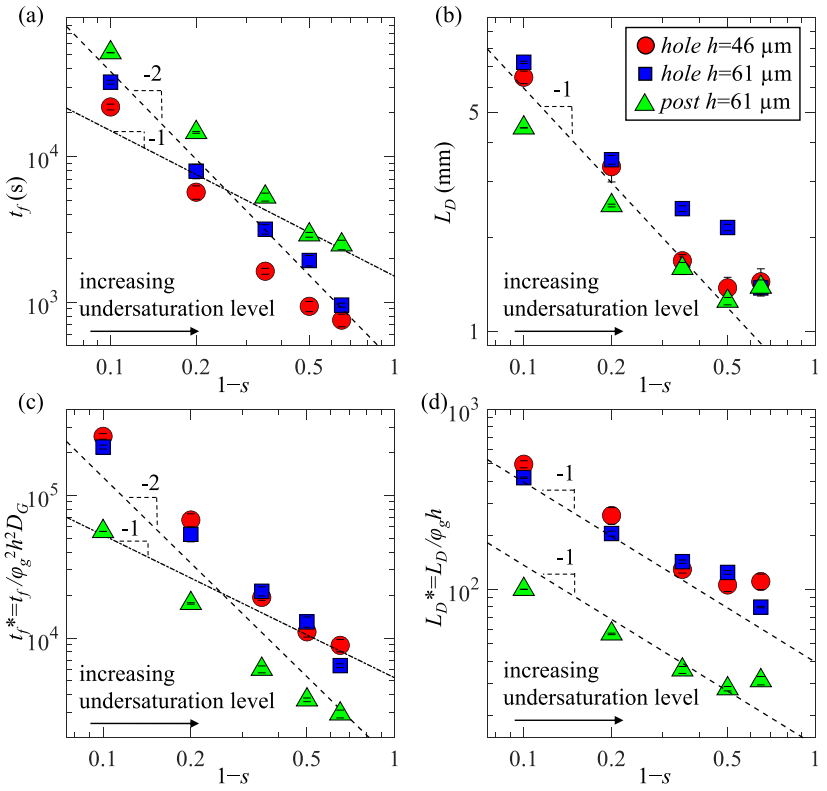

Figure 6. Experimentally measured (a) t_f, (b) L_D, (c) t_f^*, and (d) L_D^* as a function of $1 - s$ for three SHSs. The error bars are obtained by repeating the experiments under the same conditions for 2 to 4 times, and each experiment uses a fresh SHS sample of the same textures. A total of 55 experiments are performed. t_f is defined by the time when $P_{bright} = 0.1$.

Following the same definition of t_f for SHS with holes, we define the longevity for SHS with posts as the time when P_{bright} reaches a threshold value.

To study the impact of s on the wetting process, Figure 5a–c show the time-variation of P_{bright} at five different values of s for the three SHSs, respectively. Clearly, by reducing s (i.e., increasing the undersaturation level), P_{bright} decreases faster with time, indicating larger gas diffusion rates. This trend is consistent among the different SHSs.

Figure 6a shows t_f (defined based on $P_{bright} = 0.1$) as a function of $1 - s$ for the three SHSs. For comparison, the two scaling relations $t_f \sim (1 - s)^{-1}$ and $t_f \sim (1 - s)^{-2}$ proposed by Lv et al. and Bourgoun and Ling, respectively, are also plotted. Clearly, the experimental data show a good agreement with the scaling relation $t_f \sim (1 - s)^{-2}$, except for the SHS with posts at large $(1 - s)$ region, $(1 - s) > 0.5$. The reason why the SHS with posts has a different power-law scaling at $(1 - s) > 0.5$ requires further investigation. Furthermore, a comparison between the two SHSs with holes shows that the one with a greater h has a longer t_f. The reason is that for the SHS with deeper holes more air is trapped on the SHS, thereby increasing the time required for all the gas to dissolve. The SHS with posts has the longest t_f for the same reason that it traps the most amount of air. The good agreement between our experimental results and the scaling relation $t_f \sim (1 - s)^{-2}$ still holds even if a different threshold (e.g., $P_{bright} = 0.05$, 0.15, 0.2, and 0.3) is used to determine t_f (see Supporting Information Figure S1).

Next, we discuss why scaling relation $t_f \sim (1 - s)^{-2}$ better describes the SHS longevity in undersaturated water. According to Fick's first law, the mass flux of gas from SHS to liquid can be approximated as

$$J(t) = -D_G \left.\frac{\partial c}{\partial y}\right|_{SHS} \sim D_G \frac{c_i - c_\infty}{l_D} = \frac{D_G c_i}{l_D}(1 - s) \tag{2}$$

where $\partial c/\partial y|_{SHS}$ is the concentration gradient near the SHS, D_G is the diffusion coefficient, and l_D is the diffusion length at t. Assuming the total mass of gas on the SHS is m_0, the time required for all gas to dissolve (t_f) can be calculated from

$$m_0 = A\int_0^{t_f} J\,dt \sim A\int_0^{t_f} \frac{D_G c_i}{l_D}(1-s)\,dt \tag{3}$$

where A is the surface area. According to eq 3, the scaling relation $t_f \sim (1 - s)^{-1}$ is deduced by assuming l_D to be constant with respect to time, while the scaling relation $t_f \sim (1 - s)^{-2}$ is obtained by assuming the classical diffusion formula $l_D \sim (D_G t)^{0.5}$. The agreement between our experimental data and the scaling relation $t_f \sim (1 - s)^{-2}$ suggests that l_D increases with time following $l_D \sim (D_G t)^{0.5}$, and the mass flux decreases with time as $J \sim t^{-0.5}$. This is expected because during the process of gas diffusion into the liquid, the gas molecules propagate further away from the SHS and the length scale of the diffusion increases.[40−42]

To better understand the diffusion process, we define and calculate a diffusion length L_D based on the time-averaged mass flux as

$$J_{ave} = \frac{m_0}{At_f} = \frac{D_G c_i}{L_D}(1-s) \tag{4}$$

Here, we use $m_0 = \rho_{air}\lambda^2\phi_g h$, ϕ_g is the gas fraction (surface area covered by gas), $A = \lambda^2$, and $\rho_{air} = 1.3$ kg/m^3 for the density of air. The benefit of introducing L_D is that the SHS longevity can be estimated using eq 4 if L_D is known. By

https://doi.org/10.1021/acs.langmuir.3c03006
Langmuir XXXX, XXX, XXX−XXX

definition, L_D quantifies the height of the liquid column that is affected by the gas dissolution. Substituting the scaling relation $t_f \sim (1 - s)^{-2}$ into eq 4, one finds a scaling relation $L_D \sim (1 - s)^{-1}$, which is confirmed by our experimental data for SHSs of various texture geometries, as shown in Figure 6b. This result indicates that L_D decreases with increasing undersaturation level of the liquid. That is expected since as the undersaturation level increases, less volume of liquid is required to absorb the gas. In addition, comparing between the two SHSs with holes shows that the one with a greater h has a larger L_D. This trend is also expected since for the SHS with a greater h, more liquid is required to absorb all of the gas.

Considering that the mass of air trapped on the SHS per surface area is $m_0/A = \rho_{air}\phi_g h$, a dimensionless SHS longevity and a dimensionless diffusion length can be derived as $t_f^* = t_f/\phi_g^2 h^2 D_G$ and $L_D^* = L_D/\phi_g h$, respectively. Figure 6c,d shows t_f^* and L_D^*. After normalization, the results for holes and posts do not overlap, suggesting that the gas diffusion process might depend on the texture geometry. Future investigation is required to understand the scaling relations between SHS longevity and texture parameters, including texture geometry, dimension, and pattern as well as gas fraction, etc.

It should be noted that the scaling relations for SHS longevity and diffusion length as a function of the undersaturation level proposed in the current study are applicable to static conditions in a quiescent flow. Our results are useful for applications where SHS is immersed in quasi-static liquid, for example, to prevent biofouling, corrosion, and icing. However, for an SHS under flow conditions, different scaling relations might be observed. For example, in a previous work by Ling et al.,[27] they found that the diffusion length (or Sherwood number) was nearly a constant at different degrees of undersaturation. The reason might be that a steady concentration boundary layer was developed over SHS under flow conditions, and the diffusion length was governed by the thickness of the concentration boundary layer.

Furthermore, since our experiments only include SHSs with simple texture geometries, the applicability of the observed scaling relations to SHSs with more complex texture geometries or random textures requires future investigation. Nevertheless, according to the theoretical analysis, the −2 power-law scaling between t_f and $(1 - s)$ holds as long as the mass flux reduces with time as $J \sim t^{-0.5}$. We suspect that the reduction of mass flux with time is generally true regardless of the texture geometry, considering that with time the gas concentration in liquid increases and the concentration gradient reduces.

Finally, our conclusions are limited to SHS with relatively large texture sizes. For SHS with smaller texture sizes, the impact of the surface tension on the gas concentration near the gas−liquid interface is not negligible. As a consequence, as the interface deforms during the diffusion process, the value of s changes. According to our theoretical analysis in eq 3, the −2 power-law scaling between t_f and $(1 - s)$ is derived based on the assumption that s is a constant. Thus, for SHS with smaller texture sizes, one may observe a different scaling between t_f and $(1 - s)$. In particular, for SHS with nanoscale texture, the pressure in the plastron (and thus c_i) significantly reduces due to surface tension, causing the liquid to be oversaturated (i.e., $s > 1$) and stable nanoscale gas bubbles to persist.[51,52]

CONCLUSIONS

In conclusion, we studied the impact of the undersaturation level of the liquid on the SHS longevity by performing novel experimental measurements. Although it is well-known that the SHS longevity reduces with increasing undersaturation level, the scaling relation between the two terms is unclear. The main contribution of this work is that new experimental data and theoretical analysis were provided, which clarify the scaling relation between SHS longevity and the undersaturation level. Unlike earlier studies, our experimental method was not affected by pressure and immersed objective lens, allowing higher accuracy and confidence in our measurement of SHS longevity compared with those studies. Our experimental data revealed the scaling dependences of SHS longevity and diffusion length on the undersaturation level of liquid as $t_f \sim (1 - s)^{-2}$ and $L_D \sim (1 - s)^{-1}$. These scaling relations suggest that as the gas dissolves into the liquid, mass flux reduces with time as $J \sim t^{-0.5}$. We also found that SHS with a larger texture depth (or height) has a longer longevity and a longer diffusion length. Overall, our results provide a better understanding of the diffusion wetting transition of underwater SHS and how its lifetime and diffusion length change for different texture geometry characteristics under different undersaturation conditions. Future study will consider the impacts of other texture parameters (such as texture wavelength, gas fraction), nanoscale texture, and flows on the SHS longevity in undersaturated environments. It should be highlighted that the agreement of our experimental results with the power law relations does not directly prove the laws of diffusion. Future experimental studies that measure the mass flux and the gas concentration field in the liquid near the SHS are required to better understand the gas dissolution process and test the diffusion models.

ASSOCIATED CONTENT

Data Availability Statement

The data that support the findings of this study are available from the corresponding author upon reasonable request.

Supporting Information

The Supporting Information is available free of charge at https://pubs.acs.org/doi/10.1021/acs.langmuir.3c03006.

Supplementary Figure S1 (PDF)

AUTHOR INFORMATION

Corresponding Author

Hangjian Ling − *Department of Mechanical Engineering, University of Massachusetts Dartmouth, Dartmouth, Massachusetts 02747, United States;* orcid.org/0000-0001-9014-7126; Email: hling1@umassd.edu

Authors

Ali Nosrati − *Department of Mechanical Engineering, University of Massachusetts Dartmouth, Dartmouth, Massachusetts 02747, United States*

Shabnam Mohammadshahi − *Department of Mechanical Engineering, University of Massachusetts Dartmouth, Dartmouth, Massachusetts 02747, United States;* orcid.org/0000-0002-6474-9526

Mehdi Raessi − *Department of Mechanical Engineering, University of Massachusetts Dartmouth, Dartmouth, Massachusetts 02747, United States*

Complete contact information is available at:

https://doi.org/10.1021/acs.langmuir.3c03006
Langmuir XXXX, XXX, XXX−XXX

https://pubs.acs.org/10.1021/acs.langmuir.3c03006

Notes

The authors declare no competing financial interest.

■ ACKNOWLEDGMENTS

We thank the support of National Science Foundation under grant no. 2041479, UMass Dartmouth's Marine and Undersea Technology (MUST) Research Program funded by the Office of Naval Research (ONR) under grant no. N00014-20-1-2170, and Seed Funding program from the Office of the Provost at the University of Massachusetts Dartmouth.

■ REFERENCES

(1) Ling, H.; Srinivasan, S.; Golovin, K.; McKinley, G. H.; Tuteja, A.; Katz, J. High-resolution velocity measurement in the inner part of turbulent boundary layers over super-hydrophobic surfaces. *J. Fluid Mech.* **2016**, *801*, 670−703.
(2) Rothstein, J. P. Slip on Superhydrophobic Surfaces. *Annu. Rev. Fluid. Mech.* **2010**, *42*, 89−109.
(3) Xiang, T.; Han, Y.; Guo, Z.; Wang, R.; Zheng, S.; Li, S.; Li, C.; Dai, X. Fabrication of Inherent Anticorrosion Superhydrophobic Surfaces on Metals. *ACS Sustain. Chem. Eng.* **2018**, *6*, 5598−5606.
(4) Mohamed, A. M. A.; Abdullah, A. M.; Younan, N. A. Corrosion behavior of superhydrophobic surfaces: A review. *Arab. J. Chem.* **2015**, *8*, 749−765.
(5) Fadeeva, E.; Truong, V. K.; Stiesch, M.; Chichkov, B. N.; Crawford, R. J.; Wang, J.; Ivanova, E. P. Bacterial retention on superhydrophobic titanium surfaces fabricated by femtosecond laser ablation. *Langmuir* **2011**, *27*, 3012−3019.
(6) Privett, B. J.; Youn, J.; Hong, S. A.; Lee, J.; Han, J.; Shin, J. H.; Schoenfisch, M. H. Antibacterial fluorinated silica colloid superhydrophobic surfaces. *Langmuir* **2011**, *27*, 9597−9601.
(7) Zhang, P.; Lin, L.; Zang, D.; Guo, X.; Liu, M. Designing Bioinspired Anti-Biofouling Surfaces based on a Superwettability Strategy. *Small* **2017**, *13*, 1−9.
(8) Latthe, S. S.; Sutar, R. S.; Bhosale, A. K.; Nagappan, S.; Ha, C.-S.; Sadasivuni, K. K.; Liu, S.; Xing, R. Recent developments in air-trapped superhydrophobic and liquid-infused slippery surfaces for anti-icing application. *Prog. Org. Coating* **2019**, *137*, 105373.
(9) Golovin, K.; Kobaku, S. P. R.; Lee, D. H.; DiLoreto, E. T.; Mabry, J. M.; Tuteja, A. Designing durable icephobic surfaces. *Sci. Adv.* **2016**, *2*, No. e1501496.
(10) Milles, S.; Soldera, M.; Voisiat, B.; Lasagni, A. F. Fabrication of superhydrophobic and ice-repellent surfaces on pure aluminium using single and multiscaled periodic textures. *Sci. Rep.* **2019**, *9*, 13944.
(11) Zhang, C.; Zhang, W.; Du, G.; Fu, Q.; Mo, J.; Nie, S. Superhydrophobic cellulosic triboelectric materials for distributed energy harvesting. *Chem. Eng. J.* **2023**, *452*, 139259.
(12) Peng, Z.; Song, J.; Gao, Y.; Liu, J.; Lee, C.; Chen, G.; Wang, Z.; Chen, J.; Leung, M. K. H. A fluorinated polymer sponge with superhydrophobicity for high-performance biomechanical energy harvesting. *Nano Energy* **2021**, *85*, 106021.
(13) Wang, X.; Liu, Y.; Cheng, H.; Ouyang, X. Surface Wettability for Skin-Interfaced Sensors and Devices. *Adv. Funct. Mater.* **2022**, *32*, 2200260.
(14) Wang, D.; Chen, L.; Feng, X. Superhydrophobicity-mediated enhanced enzymatic kinetics and high-performance bioassays. *Droplet* **2023**, *2*, No. e51.
(15) Huang, S.; Lv, P.; Duan, H. Morphology evolution of liquid-gas interface on submerged solid structured surfaces. *Extreme Mech. Lett.* **2019**, *27*, 34−51.
(16) Mehanna, Y. A.; Sadler, E.; Upton, R. L.; Kempchinsky, A. G.; Lu, Y.; Crick, C. R. The challenges, achievements and applications of submersible superhydrophobic materials. *Chem. Soc. Rev.* **2021**, *50*, 6569−6612.
(17) Bobji, M. S.; Kumar, S. V.; Asthana, A.; Govardhan, R. N. Underwater Sustainability of the "Cassie" State of Wetting. *Langmuir* **2009**, *25*, 12120−12126.
(18) Govardhan, R. N.; Srinivas, G. S.; Asthana, A.; Bobji, M. S. Time dependence of effective slip on textured hydrophobic surfaces. *Phys. Fluids* **2009**, *21*, 052001.
(19) Poetes, R.; Holtzmann, K.; Franze, K.; Steiner, U. Metastable Underwater Superhydrophobicity. *Phys. Rev. Lett.* **2010**, *105*, 166104.
(20) Samaha, M. A.; Vahedi Tafreshi, H.; Gad-el-Hak, M. Sustainability of superhydrophobicity under pressure. *Phys. Fluids* **2012**, *24*, 112103.
(21) Dilip, D.; Jha, N. K.; Govardhan, R. N.; Bobji, M. S. Controlling air solubility to maintain "Cassie" state for sustained drag reduction. *Colloids Surf. A Physicochem.* **2014**, *459*, 217−224.
(22) Dilip, D.; Bobji, M. S.; Govardhan, R. N. Effect of absolute pressure on flow through a textured hydrophobic microchannel. *Microfluid. Nanofluidics* **2015**, *19*, 1409−1427.
(23) Hokmabad, B. V.; Ghaemi, S. Effect of Flow and Particle-Plastron Collision on the Longevity of Superhydrophobicity. *Sci. Rep.* **2017**, *7*, 41448.
(24) Samaha, M. A.; Tafreshi, H. V.; Gad-El-Hak, M. Influence of flow on longevity of superhydrophobic coatings. *Langmuir* **2012**, *28*, 9759−9766.
(25) Xu, M.; Sun, G.; Kim, C.-J. Infinite Lifetime of Underwater Superhydrophobic States. *Phys. Rev. Lett.* **2014**, *113*, 136103.
(26) Sun, W.-Y.; Kim, C.-J. The role of dissolved gas in longevity of Cassie states for immersed superhydrophobic surfaces *2013 IEEE 26th International Conference on Micro Electro Mechanical Systems (MEMS)*; IEEE, 2013, pp 397−400.
(27) Ling, H.; Katz, J.; Fu, M.; Hultmark, M. Effect of Reynolds number and saturation level on gas diffusion in and out of a superhydrophobic surface. *Phys. Rev. Fluid* **2017**, *2*, 124005.
(28) Lv, P.; Xue, Y.; Shi, Y.; Lin, H.; Duan, H. Metastable States and Wetting Transition of Submerged Superhydrophobic Structures. *Phys. Rev. Lett.* **2014**, *112*, 196101.
(29) Li, X.; Wang, Y.; Zeng, B.; Li, Y.; Tan, H.; Zandvliet, H. J. W.; Zhang, X.; Lohse, D. Entrapment and Dissolution of Microbubbles Inside Microwells. *Langmuir* **2018**, *34*, 10659−10667.
(30) Xiang, Y.; Huang, S.; Lv, P.; Xue, Y.; Su, Q.; Duan, H. Ultimate Stable Underwater Superhydrophobic State. *Phys. Rev. Lett.* **2017**, *119*, 134501.
(31) Xiang, Y.; Xue, Y.; Lv, P.; Li, D.; Duan, H. Influence of fluid flow on the stability and wetting transition of submerged superhydrophobic surfaces. *Soft Matter* **2016**, *12*, 4241−4246.
(32) Checco, A.; Ocko, B. M.; Rahman, A.; Black, C. T.; Tasinkevych, M.; Giacomello, A.; Dietrich, S. Collapse and reversibility of the superhydrophobic state on nanotextured surfaces. *Phys. Rev. Lett.* **2014**, *112*, 216101−216105.
(33) Kim, H.; Park, H. Diffusion characteristics of air pockets on hydrophobic surfaces in channel flow: Three-dimensional measurement of air-water interface. *Phys. Rev. Fluid* **2019**, *4*, 074001.
(34) Karatay, E.; Tsai, P. A.; Lammertink, R. G. H. Rate of gas absorption on a slippery bubble mattress. *Soft Matter* **2013**, *9*, 11098−11106.
(35) Emami, B.; Hemeda, A. A.; Amrei, M. M.; Luzar, A.; Gad-el-Hak, M.; Vahedi Tafreshi, H. Predicting longevity of submerged superhydrophobic surfaces with parallel grooves. *Phys. Fluids* **2013**, *25*, 062108.
(36) Hemeda, A. A.; Gad-el-Hak, M.; Tafreshi, H. V. Effects of hierarchical features on longevity of submerged superhydrophobic surfaces with parallel grooves. *Phys. Fluids* **2014**, *26*, 082103.
(37) Piao, L.; Park, H. Two-Dimensional Analysis of Air-Water Interface on Superhydrophobic Grooves under Fluctuating Water Pressure. *Langmuir* **2015**, *31*, 8022−8032.
(38) Flynn, M. R.; Bush, J. W. M. Underwater breathing: The mechanics of plastron respiration. *J. Fluid Mech.* **2008**, *608*, 275−296.
(39) Hemeda, A. A.; Tafreshi, H. V. General formulations for predicting longevity of submerged superhydrophobic surfaces composed of pores or posts. *Langmuir* **2014**, *30*, 10317−10327.

(40) Kadoko, J.; Karamanis, G.; Kirk, T.; Hodes, M. One-Dimensional Analysis of Gas Diffusion-Induced Cassie to Wenzel State Transition. *J. Heat Transfer* **2017**, *139*, 1−10.
(41) Bourgoun, A.; Ling, H. A General Model for the Longevity of Super-Hydrophobic Surfaces in Under-Saturated, Stationary Liquid. *J. Heat Transfer* **2022**, *144*, 042101.
(42) Mayer, M. D.; Kadoko, J.; Hodes, M. Two-Dimensional Numerical Analysis of Gas Diffusion-Induced Cassie to Wenzel State Transition. *J. Heat Transfer* **2021**, *143*, 103001.
(43) Haase, A. S.; Karatay, E.; Tsai, P. A.; Lammertink, R. G. H. Momentum and mass transport over a bubble mattress: the influence of interface geometry. *Soft Matter* **2013**, *9*, 8949.
(44) Chellam, S.; Wiesner, M. R.; Dawson, C. Slip at a uniformly porous boundary: effect on fluid flow and mass transfer. *J. Eng. Math.* **1992**, *26*, 481−492.
(45) Barth, C.; Samaha, M.; Tafreshi, H.; Gad-el-Hak, M. Convective Mass Transfer From Submerged Superhydrophobic Surfaces: Turbulent Flow. *Int. J. Flow Control* **2013**, *5*, 143−152.
(46) Arunachalam, S.; Ahmad, Z.; Das, R.; Mishra, H. Counter-intuitive Wetting Transitions in Doubly Reentrant Cavities as a Function of Surface Make-Up, Hydrostatic Pressure, and Cavity Aspect Ratio. *Adv. Mater. Interfaces* **2020**, *7*, 1−13.
(47) Zheng, Q.-S.; Yu, Y.; Zhao, Z.-H. Effects of Hydraulic Pressure on the Stability and Transition of Wetting Modes of Super-hydrophobic Surfaces. *Langmuir* **2005**, *21*, 12207−12212.
(48) Nosonovsky, M. Multiscale roughness and stability of superhydrophobic biomimetic interfaces. *Langmuir* **2007**, *23*, 3157−3161.
(49) Battino, R.; Rettich, T. R.; Tominaga, T. The Solubility of Nitrogen and Air in Liquids. *J. Phys. Chem. Ref. Data* **1984**, *13*, 563−600.
(50) Moulinet, S.; Bartolo, D. Life and death of a fakir droplet: Impalement transitions on superhydrophobic surfaces. *Eur. Phys. J. E* **2007**, *24*, 251−260.
(51) Lohse, D.; Zhang, X. Pinning and gas oversaturation imply stable single surface nanobubbles. *Phys. Rev. E: Stat., Nonlinear, Soft Matter Phys.* **2015**, *91*, 031003.
(52) Weijs, J. H.; Lohse, D. Why Surface Nanobubbles Live for Hours. *Phys. Rev. Lett.* **2013**, *110*, 054501.

https://doi.org/10.1021/acs.langmuir.3c03006
Langmuir XXXX, XXX, XXX−XXX